


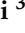







Article

The Role of Vegetation on Urban Atmosphere of Three European Cities—Part 1: Evaluation of Vegetation Impact on Meteorological Conditions

Massimo D'Isidoro ^{1,†}, Mihaela Mircea ^{1,*,†}, Rafael Borge ², Sandro Finardi ³, David de la Paz ², Gino Briganti ¹, Felicita Russo ¹, Giuseppe Cremona ¹, Maria Gabriella Villani ¹, Mario Adani ¹, Gaia Righini ¹, Lina Vitali ¹, Milena Stracquadiano ¹, Rossella Prandi ⁴ and Giuseppe Carlino ⁴

¹ Laboratory of Atmospheric Pollution, Italian National Agency for New Technologies, Energy and Sustainable Economic Development—ENEA, 40129 Bologna, Italy; massimo.disidoro@enea.it (M.D.); gino.briganti@enea.it (G.B.); felicita.russo@enea.it (F.R.); giuseppe.cremona@enea.it (G.C.); mariagabriella.villani@enea.it (M.G.V.); mario.adani@enea.it (M.A.); gaia.righini@enea.it (G.R.); lina.vitali@enea.it (L.V.); milena.stracquadiano@enea.it (M.S.)

² Department of Chemical and Environmental Engineering, ETSII—Universidad Politécnica de Madrid (UPM), 28040 Madrid, Spain; rafael.borge@upm.es (R.B.); david.delapaz@upm.es (D.d.l.P.)

³ ARIANET, 20159 Milan, Italy; s.finardi@aria-net.it

⁴ SIMULARIA S.r.l., Via Sant'Antonio da Padova 12, 10121 Turin, Italy; r.prandi@simularia.it (R.P.); g.carlino@simularia.it (G.C.)

* Correspondence: mihaela.mircea@enea.it

† These two authors contributed equally to this work.

Abstract: This study quantifies the vegetation impact on urban meteorology by means of the numerical model WRF (Weather Research and Forecasting model). The assessment was made for two months: July and January. These were considered as representative for the summer and winter seasons, for the reference year 2015 in three European cities: Bologna, Milano, and Madrid. Two simulations at 1 km resolution were conducted over the cities with and without the actual urban vegetation, called VEG and NOVEG, respectively, in the model input. Then, the impact of vegetation was evaluated as the difference between the two simulations (VEG-NOVEG) for temperature, relative humidity, and wind speed fields. In general, we found that, as can be expected, urban vegetation tends to cool the atmosphere, enhance the humidity, and reduce the wind speed. However, in some cases, areas with the opposite behaviour exist, so that no a priori results can be attributed to the presence of urban vegetation. Moreover, even when major impact is confined around grid cells where urban vegetation is present, changes in meteorological quantities can be observed elsewhere in the city's area. The magnitude of urban vegetation impact is higher in summer than in winter and it depends on the city's morphological peculiarities, such as urban texture and vegetation types and distribution: average July temperature variations due to the presence of urban vegetation reach peaks of -0.8 °C in Milano, -0.6 °C Madrid, and -0.4 °C in Bologna, while in January, the values range between -0.3 and -0.1 °C. An average heating effect of ca. $+0.2$ °C is found in some parts of Madrid in January. For relative humidity, we found increments of 2%–3% in July and 0.5%–0.8% in January, while a decrease in wind speed was found between 0.1 and 0.5 m/s, with the highest occurring in Madrid during July.

Keywords: urban vegetation; urban heat island; urban meteorology; WRF; atmospheric modelling



Citation: D'Isidoro, M.; Mircea, M.; Borge, R.; Finardi, S.; de la Paz, D.; Briganti, G.; Russo, F.; Cremona, G.; Villani, M.G.; Adani, M.; et al. The Role of Vegetation on Urban Atmosphere of Three European Cities—Part 1: Evaluation of Vegetation Impact on Meteorological Conditions. *Forests* **2023**, *14*, 1235. <https://doi.org/10.3390/f14061235>

Academic Editor: Manuel T. Lerdau

Received: 15 May 2023

Revised: 1 June 2023

Accepted: 12 June 2023

Published: 14 June 2023



Copyright: © 2023 by the authors. Licensee MDPI, Basel, Switzerland. This article is an open access article distributed under the terms and conditions of the Creative Commons Attribution (CC BY) license (<https://creativecommons.org/licenses/by/4.0/>).

1. Introduction

The urban heat island (UHI) is the typical microclimate regime of dense urban areas, characterised by higher temperatures, leading to uncomfortable conditions for residents, compared to the less-urbanised surroundings. Moreover, in the last few decades, ongoing climate change has aggravated the UHI effects due to an increase in heat wave (HW)

frequency, duration, and strength at the global level [1]. Similar results were found by [2], including an expansion of the heat wave season, considering 50 large metropolitan areas across the US. In Europe, ref. [3] investigated past HWs, estimating their frequency in the next few decades induced by global warming, finding an increased probability of extreme temperatures episodes in the period 2021–2040.

The UHI conditions can also affect people's health, especially in the presence of pre-existing cardiovascular and respiratory illnesses, leading to an increase in heat-related mortality [4]. In Europe, more than 70,000 fatalities were estimated from the 2003 heat wave [5], while [6] studied temperature-related extreme events, finding that HWs are the major cause for deaths. Ref. [7] estimated future heat-related mortality in the Eastern US, finding the greatest impact in many of the most urbanised counties. Many other studies can be found at national and local levels, e.g., in Germany [8], Czech Republic [9], in Italy including Rome [10], Istanbul [11], and Athens [12].

To face these effects and their worsening trend in a climate-changing environment, it is crucial for local communities and governments to evaluate, plan, and implement mitigation measures, especially in urban areas. In this respect, the use of numerical modelling capable of describing the urban environment and its interactions with atmospheric dynamics and thermodynamics represents a valid tool to support decision makers and stakeholders. Among different approaches, several studies based on the use of high-resolution (1 km or more) atmospheric models to quantify UHI are reported [13]. The Weather Research and Forecasting (WRF) model [14,15] coupled with different urban parameterizations was widely used in reproducing the urban meteorology, e.g., in Hong Kong [16], Chicago [17], Barcelona [18], Chennai [19], Beijing [20], Berlin [21], and Athens [22]. In addition to good UHI modelling, mitigation approaches need to be based on some effectiveness evidence to be successfully implemented. Within cities, so-called Nature-Based Solutions (NBSs) can be a valid instrument to mitigate UHI effects, especially those involving vegetation [23–25]. A major role is played by urban trees whose shadowing effect contributes to lower temperature peaks cooling the air [26–28].

This work presents some of the results obtained in the framework of the EU-funded VEG-GAP Life project (<https://www.lifeveggap.eu>, accessed on 15 May 2023), quantifying the effects of current urban vegetation on meteorological conditions in three selected cities in Southern Europe having different extensions, morphology, and populations, Bologna (141 km², population ca. 400,000), Milano (181 km², population ca. 1,400,000), and Madrid (605 km², population ca. 3,150,000), which can be considered as representative of small-, medium- and large-sized European cities, respectively. In a companion paper to Mircea et al. (2023) [29], we extensively address the impact of urban vegetation on air quality in these three cities, using the meteorological data produced in this work. In spite of the continuous reduction in anthropogenic emissions from 1990, the concentration of some pollutants in European cities is still high; therefore, it is necessary to understand and quantify the role of vegetation in cleaning the air through its impact on meteorology. Here, and in the companion paper, the investigations are made with numerical models, as suggested by the Air Quality Directive (Directive 2008/50/EC, <https://eur-lex.europa.eu/legal-content/en/ALL/?uri=CELEX:32008L0050>, accessed on 11 June 2023).

Section 2 contains a description of the modelling setup used for simulating meteorological conditions in the three cities, together with a description of urban vegetation and urban morphology used as input in the simulations. The results are presented in Section 3. All the simulations were carried out with the WRF model with two different versions, one for Italian cities and one for the Spanish city, and partly different configurations in describing the atmospheric processes.

2. Materials and Methods

In this investigation we chose the year 2015, the 4th warmest year globally according to NOAA [30], when one of the worst HWs on record hit Europe [31,32], with relevant impact on heat-induced mortality across the continent [8,9]. Moreover, in 2015, Madrid experienced the longest HW of 24 days [33].

This choice allowed us to test our methodology in extremely warm conditions that are more and more frequently happening (<https://climate.copernicus.eu/climate-indicators/temperature>; <https://www.epa.gov/climate-indicators/climate-change-indicators-heat-waves>, accessed on 11 June 2023 [34]), with global temperatures expected to reach new records in the next five years (2023–2027) according to World Meteorological Organization (WMO) Global Annual to Decadal Climate Update [35].

To assess the impact of urban vegetation on meteorology, the WRF atmospheric model was used [14,15]. WRF is a state-of-the-art atmospheric numerical model based on fully compressible, Eulerian non-hydrostatic equations, on terrain following hybrid levels with constant pressure surface as top of the model boundary. It is capable of simulating the whole dynamics and thermodynamics of the atmosphere, giving the possibility to choose among several parameterisation options for processes, such as radiation, microphysics, surface layer, land surface model, and planetary boundary layer. The model can adopt different nesting methods depending on the user choice: one-way, two-way, and moving nesting options can be selected.

For this work, two simulations (VEG and NOVEG) for the whole year 2015 were performed focussing on the three European cities Bologna, Milano, and Madrid (Figure 1), considering computational grids having 1 km horizontal resolution. Except for urban vegetation input data, both simulations share the same settings and inputs, including a two-dimensional description of sub-grid distribution of urban fraction (3 urban classes were considered for Milano and Bologna and 6 for Madrid; more details are provided in Section 2.2). The difference between VEG and NOVEG resides in the definition of vegetation fraction within the cells where urban fraction prevails, hereafter called “urban vegetation” and “urban cells”, respectively. In VEG simulation, we considered the actual urban vegetation distribution, thus reproducing the meteorological conditions impacted by the present land cover conditions over the cities, while in NOVEG simulation, the urban vegetation was replaced with barren soil to simulate the meteorological evolution of 2015 as if urban vegetation was absent. It is worth noting that, for both simulations, actual vegetation was used in non-strictly urban cells, that is, in cells where vegetation fraction prevails over urban fraction (hereafter named “vegetation cells”). Moreover, for NOVEG simulation over Madrid, urban vegetation was replaced by barren soil only in the urban cells located within municipality and containing urban trees and green spaces in the VEG simulation, leaving unchanged urban cells containing uncultivated areas, dryland cropland, or pastures, e.g., in peripheral or dismissed industrial areas (this treatment was suitable to model Madrid’s peculiar land cover features; more details in Section 2.2 and in [36]). On the other hand, in the case of Bologna and Milano, each urban cell of the domains was affected. Models’ configurations over cities at 1 km resolution are described in Section 2.1, while more details on vegetation types present in the three cities and their spatial distribution can be found in Figure S1 and Table S3 in the Supporting Information of the companion paper [29].

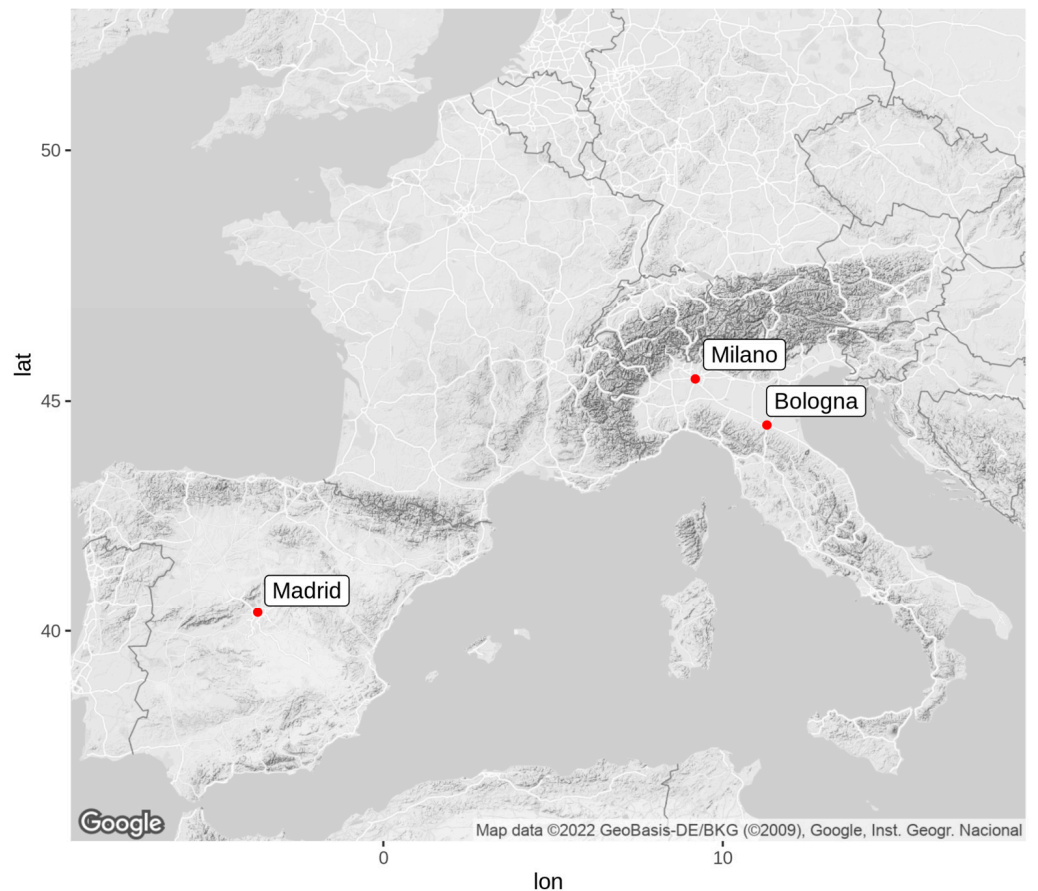


Figure 1. Location of the three cities. Map source: Google Maps.

2.1. Models and Parameterisations

To produce VEG and NOVEG simulations over cities in Italy and Spain, the WRF model was run using similar settings. The configurations used for the high-resolution domains (1 km) are reported in Table 1, while a description of coarser-resolution nested domains used to perform the simulations is available in Table S1 in the Supporting Information (SI). The simulation settings were defined after performing sensitivity tests on computational grids (domain extensions, resolution, and vertical level definition). Moreover, the differences between the two versions of WRF used in the present study (v3.9.1.1 [15] for Italian cities and v4.1.2 [14] for Madrid) are less relevant than the choice of physical schemes. Furthermore, due to the comparative nature of this study, three aspects are the most relevant: a good reproduction of the meteorological phenomena verified with measured data, the possibility to include vegetation information in a similar way, and the morphology of the city.

To improve the model performance in urban environment, the 100 m resolution CORINE land cover [37] was adopted. In this scope, the 22 CORINE categories were reclassified according to the 33 US Geological Survey (USGS) considered in WRF, following the approach described in Section 2.2. Moreover, a multi-layer urban canopy model, the Building Effect Parameterization (BEP; [38]), was activated in both WRF systems. The BEP scheme builds its own “urban grid”, with up to 18 vertical levels to describe the impact of urban structure on airflow and considering the urban and vegetation type and fraction within the grid cell.

In addition to surface properties (albedo, heat capacity, emissivity, etc.) needed by the standard WRF version, the application of the BEP urban parametrization requires some details regarding the urban morphology (height of buildings, street width, etc.) for each urban category and for each city. This information comes from high-resolution public cartographic

databases (National Cartographic portal for Italian cities, <http://www.pcn.minambiente.it/mattm/>, accessed on 11 June 2023; Autonomous body National Center for Geographic Information, <https://centrodedescargas.cnig.es> for Madrid, accessed on 11 June 2023) that were statistically analyzed within administrative city’s boundaries through a geographic information system (GIS). In Table 2a,b, relevant input BEP parameters estimated for the three cities are shown.

Table 1. Description of models’ setup over Italy (Milano and Bologna) and Spain (Madrid).

Modelling Setup	Italy (Milan, Bologna)	Spain (Madrid)
Model	WRF v3.9.1.1 [15]	WRFv4.1.2 [14]
PROCESSES		
Microphysics	WRF Single Moment 6-class scheme [39]	WRF Single Moment 6-class scheme [39]
Cumulus Parameterization	Off	Off
PBL Scheme	Mellor Yamada Janjic (MY); [40]	Bougeault-Lacarrère PBL (BOULAC; [41])
Surface layer	Monin-Obukhov/Janjic Eta [42]	Monin-Obukhov/Janjic Eta [42]
Urban Parameterization	BEP [38]	BEP [38,43]
Land Surface	Noah LSM (Land Surface Model, [44])	Noah LSM (Land and Surface Model, [44])
Longwave Radiation	RRTMG [45]	GFDL [46]
Shortwave Radiation	RRTMG [45]	MM5 Dudhia [47]
Landuse database	Corine Land Cover 2012 (mapped to USGS 33 classes)	Corine Land Cover 2012 (mapped to USGS 33 classes)
Number of vertical layers	41	39
Vertical extent	25,000 m	17,600 m
Horizontal resolution	1 km	1 km

Table 2. (a) BEP relevant inputs: street and building width for the three urban categories. Units in m. (b) BEP relevant inputs: building fractions for the three urban categories as a function of height classes.

(a)				
Urban Categories	Parameters	Bologna	Madrid	Milan
Low density residential	Street Width	13	20	15
	Building Width	31	20	28
High density residential	Street Width	12	25	20
	Building Width	40	17	25
Commercial	Street Width	18	30	25
	Building Width	64	13	53
(b)				
City	Building Height (m)	Low Density Residential (%)	High Density Residential (%)	Commercial (%)
Bologna	5	8	2	10
	10	29	11	57
	15	27	42	23
	20	21	29	5
	25	8	11	2
	30	5	3	2
	35	2	2	1

Table 2. Cont.

(b)				
City	Building Height (m)	Low Density Residential (%)	High Density Residential (%)	Commercial (%)
Madrid	5	4	3	15
	10	11	6	22
	15	59	18	38
	20	8	15	12
	25	12	27	7
	30	3	13	3
	35	3	18	3
Milan	5	19	11	15
	10	32	19	59
	15	14	14	15
	20	13	24	5
	25	10	17	3
	30	6	9	1
	35	6	6	2

2.2. Input Data

Hereafter, a detailed description of input data to WRF is given, particularly focussing on how vegetation and urban fraction layers were produced.

2.2.1. Boundary and Initial Conditions

WRF simulations at 1 km resolution (settings detailed in Table 1) were obtained through consecutive nesting from coarser domains. Concerning Bologna and Milano, two 2-way nested domains at 12 and 4 km resolution were used before the final 1-way nesting to 1 km, while the target simulation over Madrid was obtained adopting three 2-way nested grids at 27, 9, and 3 km resolution, respectively, before performing the final 1-way nesting simulation at 1 km resolution. Both modelling chains made use of ERA-5 reanalysis [48] at the boundary of their respective coarser domain. More detailed information on the WRF computational domains is provided in SI (Figure S1 and Table S1).

2.2.2. Urban and Vegetation Types and Distribution

The urban-type description requested by BEP parameterisation was obtained by remapping the classes of the Corine Land Cover into the WRF/BEP urban classification, using the following correspondence scheme: 111 (continuous urban fabric) into 32 (high-intensity residential); 112 (discontinuous urban fabric) into 31 (low-intensity residential); 12X (industrial or commercial units, road and rail networks and associated land, port areas, airports), 13X (mineral extraction sites, dump sites, construction sites) and 142 sport and leisure facilities into 33 (commercial/industrial); 141 (green urban areas) into 15 (mixed Forest). A dataset of urban classes in geographic coordinates at 3'' (≈ 100 m) was built in the format accepted by WRF pre-processor of geographic data GEOGRID. The geographic area covered by the urban dataset is coincident with that covered by Corine Land Cover classification. The standard application of WRF pre-processor allows one to obtain the urban class distribution on the simulation domains at the required spatial resolution.

Vegetation in urban areas is poorly detailed in all the land cover datasets included in WRF software releases mentioned in Table 1 and even in the Corine Land Cover, which describes major urban park areas but does not consider the presence of street trees and small gardens. The surface cover description was, therefore, improved to achieve reliable mapping of urban vegetation and a better definition of the urban fraction that can be associ-

ated with each urban cell. Municipal public green inventories, including the description of each tree species and main features, were integrated with regional forest map to improve CORINE Land Cover. The plant functional type and total vegetation fraction were then derived integrating the species-specific grid-dependent vegetation cover. Figure 2 shows a magnification of the three WRF domains with the prevalent urban class (top) and the vegetation fraction (bottom) at every grid point.

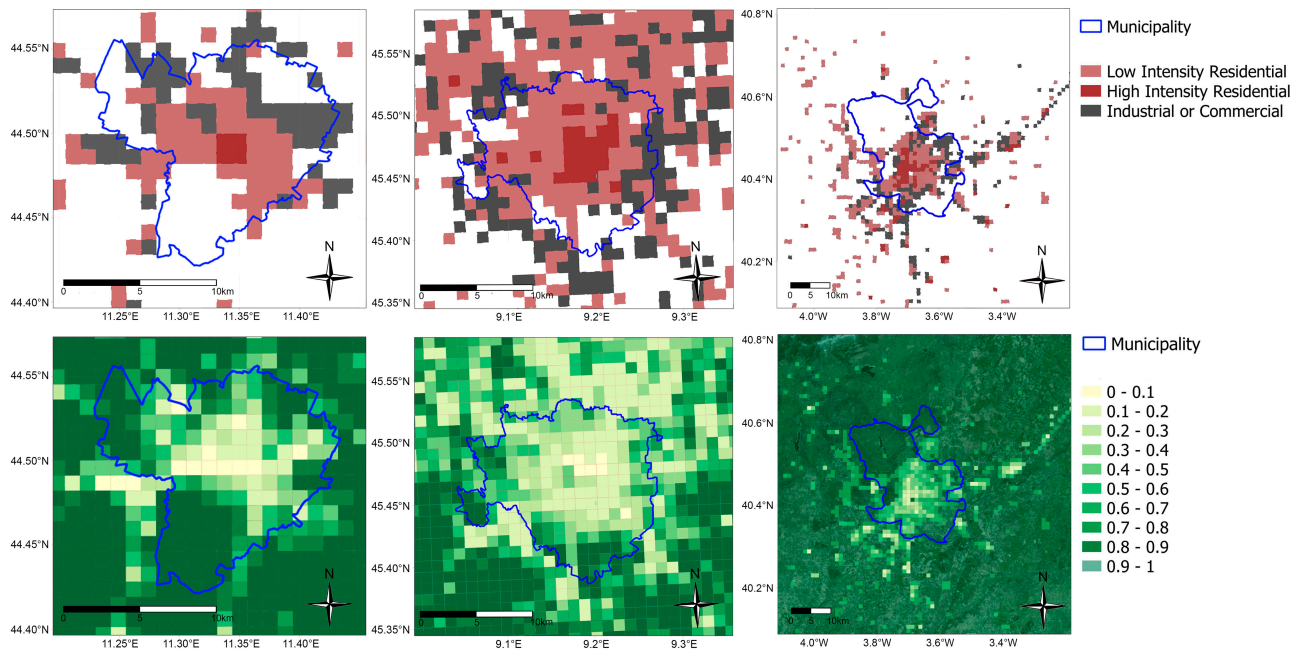


Figure 2. Distribution of the three urban categories prevalence (top row) and vegetation fraction (bottom row) on the WRF grid cells zoomed in over Bologna (left), Milano (centre), and Madrid (right). Pale red, red, and grey colours in top row indicate low-density residential, high-density residential, and commercial/industrial classes, respectively. The vegetation fraction is shown by a green palette, where dark green indicates highest values. Note the different dimensions of the cities where the same scale bar indicates a 10 km distance in each plot.

Moreover, to take advantage of detailed information over Madrid and to more realistically describe different urban vegetation types, we added new urban land use classes (34 to 36) in parallel to the three original ones (31 to 33) to represent vegetation type within the non-urban cells (more details in [43]).

In the Supporting Information of the companion paper, Mircea et al. (2023) [29], the reader can find a more detailed insight for which are the most relevant tree species present (Table S3) and the fractional land cover maps of different vegetation species (Figure S3) for the three cities.

2.3. Evaluation Approach

To compare the effect of current urban vegetation on meteorological conditions in the three cities, we considered some relevant meteorological parameters, such as temperature (T), relative humidity (RH), and wind speed (WS), near the ground. For sake of simplicity and without loss of generality, we present the results for two representative winter (January) and summer (July) months in terms of differences in the above-mentioned quantities between the two simulations: VEG-NOVEG. Other quantities, such as latent and sensible heat fluxes (LHFs and SHFs), that can be related to convective turbulence and stability are presented in SI. Moreover, the reader can refer to [29] for additional considerations regarding the effect of urban vegetation on the Planetary Boundary Layer Height (PBLH), which has an important impact on air quality.

In SI (Table S2), an extensive validation of the model against observed parameters is presented, finding WRF simulations reasonably good and generally in line with the benchmarks suggested in the literature [49,50].

All analyses and plots presented here were performed using R Statistical Software (v4.0.3; [51]) together with AirVeg (<https://gitlab.com/simularia/veg-gap/airveg>, accessed on 11 June 2023) and Tidyverse [52] packages.

3. Results and Discussion

Figures 3 and 4 show the average difference in VEG–NOVEG simulations computed from WRF hourly outputs for T (top row), RH (middle row), and WS (bottom row), referring to Bologna (left column), Milano (middle column), and Madrid (right column), for July and January, respectively. Firstly, it is worth mentioning that in Madrid, the spatial distribution of the differences roughly residing within the municipality arises from the fact that vegetation areas located outside the municipality boundaries were left unchanged in the NOVEG simulation for this city, as mentioned in Section 2.

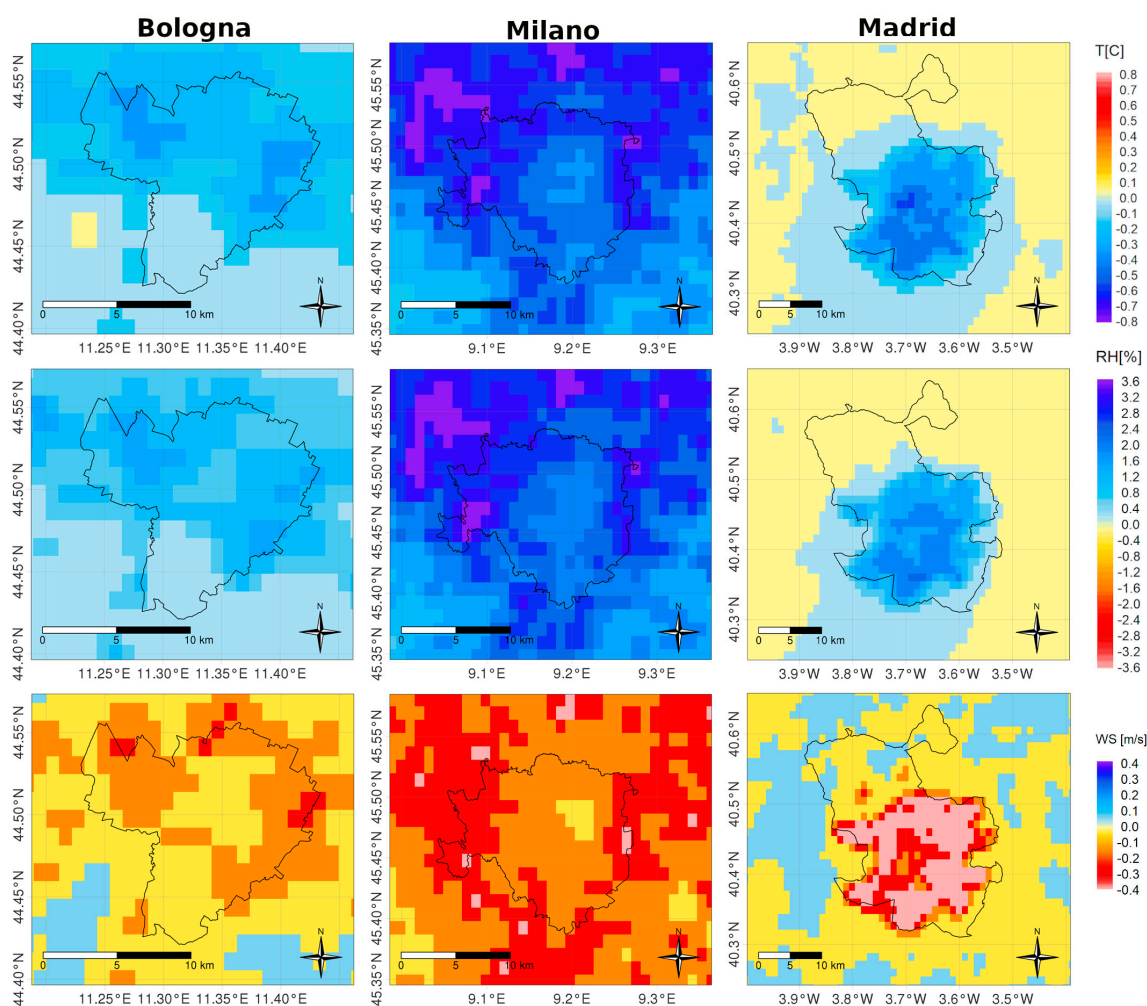


Figure 3. Average difference (VEG–NOVEG) in July for T (top row), RH (middle row), and WS (bottom row) referred to Bologna (left column), Milano (middle column), and Madrid (right column).

In Figures 3 and 4, negative values indicate that, on average, the presence of urban vegetation results in lower T, RH, and WS, while positive values indicate the opposite. In general, it is worth noting that the impact clearly depends on the city and the season. Moreover, the patterns tend to be correlated with the vegetation distribution in the urban cells (see Figure 2), from which vegetation was removed in the NOVEG simulations. This

fact is especially evident in July, indicating a more active role of vegetation in summer than in winter. This is also suggested by looking at LHF and SHF differences, which are strictly related to the presence of vegetation and spatial distribution, finding more pronounced variations in July than in January (maps in Figures S2 and S3).

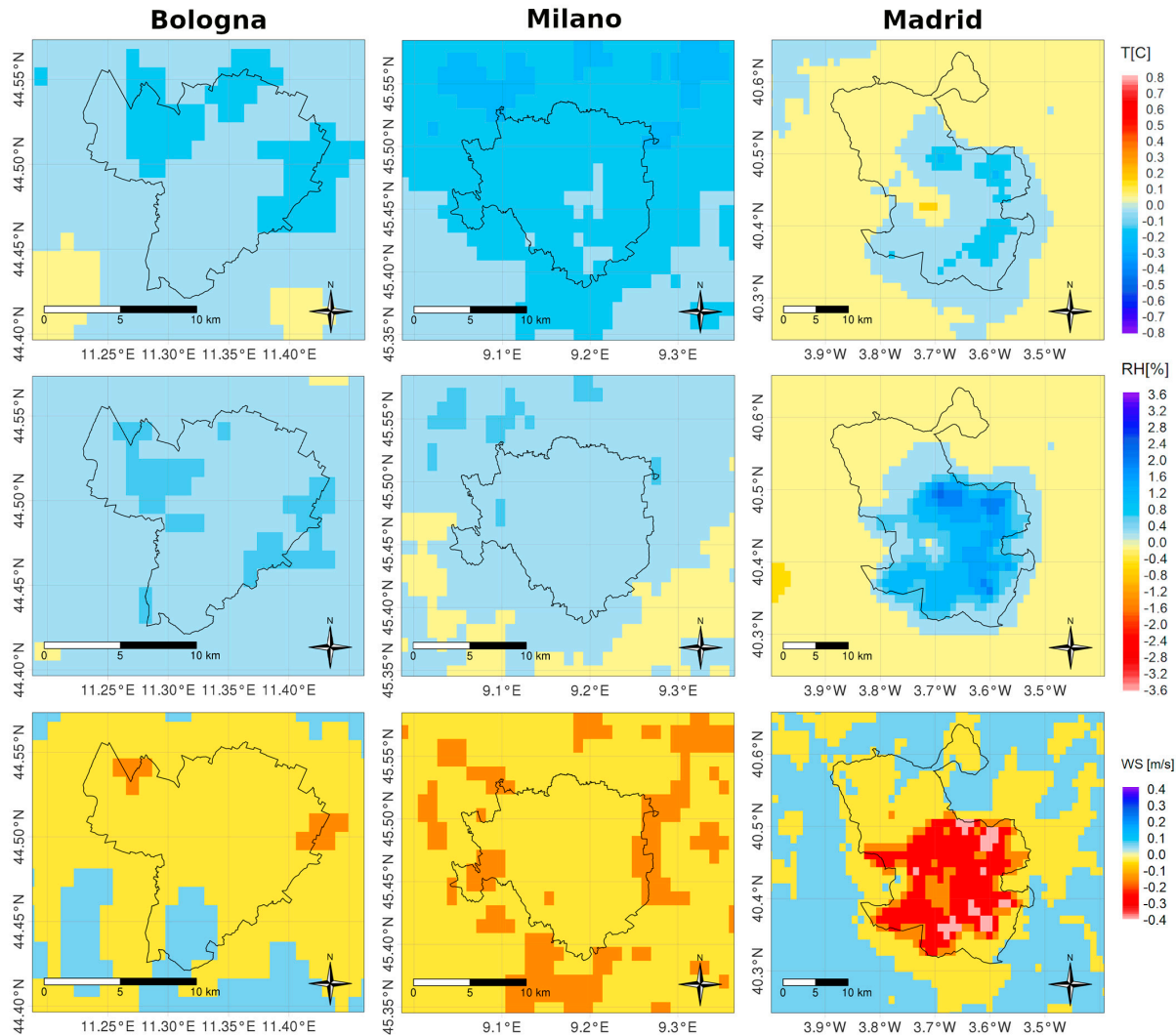


Figure 4. Same as in Figure 3 but referring to January.

Focussing on the single quantities, we note that for temperature in July (Figure 3, top row), a cooling effect is dominant, and the major differences occur in the two largest cities, Milano (up to -0.8 °C month average) and Madrid (up to -0.6 °C), while in Bologna, the maximum average cooling reaches -0.4 °C. In Madrid, the cooling effect does not extend far towards the north part of the municipality, where vegetation-dominated cells prevail over urban dominated ones (see Figure 2), meaning that vegetation was not removed in the NOVEG simulation. In January, the effect of urban vegetation on temperature is less pronounced (Figure 4, top row), with a resulting maximum cooling effect ranging from ca. -0.2 °C in Milano to -0.15 °C ÷ -0.25 °C in Bologna and Madrid, respectively. It is worth noting that in Madrid, an average warming effect of 0.1 °C ÷ 0.2 °C is present in some grid points inside the city (Figure 4, top row, right column). This result suggests that no overall cooling effect can be expected within the cities due to the presence of urban vegetation, and an opposite sign signal may result in limited areas.

Coherently with the changes observed in temperature, the presence of urban vegetation tends to increase the monthly average RH (positive values in the Figures, middle row), around 1% in July (Figure 3, highest values in Milano, up to 3%) and to ca. 1% in

January in Madrid, when Bologna and Milano increments reach maximum values around 0.8% and 0.5%, respectively (Figure 4). The rise of RH due to vegetation is attributable, in addition to lower temperatures, to the evaporation/transpiration processes associated with the presence of vegetation that tends to locally increase the atmospheric humidity; this is also evident in the LHF increment shown in the SI (Figure S2).

As expected, the presence of urban vegetation reduces wind speed by generating mechanical turbulence given to higher roughness length. This is highlighted both in July and January by negative values on the maps (Figures 3 and 4, bottom row). Wind speed differences are found to be higher in July than in January and range from -0.5 m/s to -0.1 m/s, with the highest values recorded in Madrid; this may depend on differences in the city morphologies and vegetation types and distribution but also on the meteorological conditions characterizing the city locations. Indeed, it is worth mentioning that the Po Valley, where Bologna and Milano are located, is characterised by low wind speed regimes, especially during winter, when stagnation conditions often occur, also causing air pollution peaks [53,54]. The higher variation detected in Madrid during winter for RH, WS, and surface fluxes suggests a significant impact of the vegetation composition. Ref. [36] estimated that Madrid trees have 13% of evergreen needleleaf trees and 2% of evergreen broadleaf trees, which can explain why the vegetation impact on humidity and latent heat flux remains more significant during the winter than in Bologna and Milano where deciduous species are largely dominant.

Figures 3 and 4 show that, in general, the effect of urban vegetation on meteorology depends on the city and the season, and maximum differences are confined around urban vegetation cells (patterns in Figures 3 and 4 to be compared to those in Figure 2). Nonetheless, a discernible impact, although lower, can be observed in other areas by looking in detail at the temporal variations. Focussing on temperature only (RH and WS are available in SI), Figure 5 shows the daily cycle of the median of temperature difference calculated separately over urban cells and vegetation cells located within the municipality borders of Bologna, Milano, and Madrid (left, middle, and right columns, respectively). Blue curves refer to January and red ones to July, while the corresponding shaded areas encompass the interval between the 90th and 10th percentiles. We recall that urban/vegetation cells are grouped according to the prevalence of urban/vegetation type in the land use database following the USGS classification.

In January, at midday, the difference in VEG-NOVEG tends to be positive in some cases, with a more pronounced signal in urban cells. This occurs for the median in Madrid (blue curve, right column), indicating a heating effect of vegetation in some urban cells, from which vegetation was removed in the NOVEG simulation. A possible role in this local heating could be played by latent heat release due to the presence of urban vegetation (see Figure S2). In July, the trend is similar (red curves), with a more pronounced daily cycle amplitude with respect to January. During the night, air is cooled due to the presence of vegetation in urban cells, even more than 1 °C in Milano (middle column), while the heating effect is observed in some cases during the daytime hours, especially in Madrid and Bologna. For the three cities in July, some negative and positive peaks appear in the second part of the day, when convective turbulence is fully developed. These features are probably associated with diurnal summer local circulation patterns, causing advection from other parts of the city area. It is worth noting that in the case of Milano (middle column), only a small difference in temperature variations between urban and vegetation cells is present, both in January and July. This behaviour denotes that the effect of urban vegetation tends to spread over all the cells in the municipality, with local fluctuations not strictly correlated with the local vegetation cover density. A possible explanation may be related to the fact that in Milano, urban cells outnumber vegetation cells (184 vs. 45 points), so that the urban “forcing” is stronger and propagates more effectively.

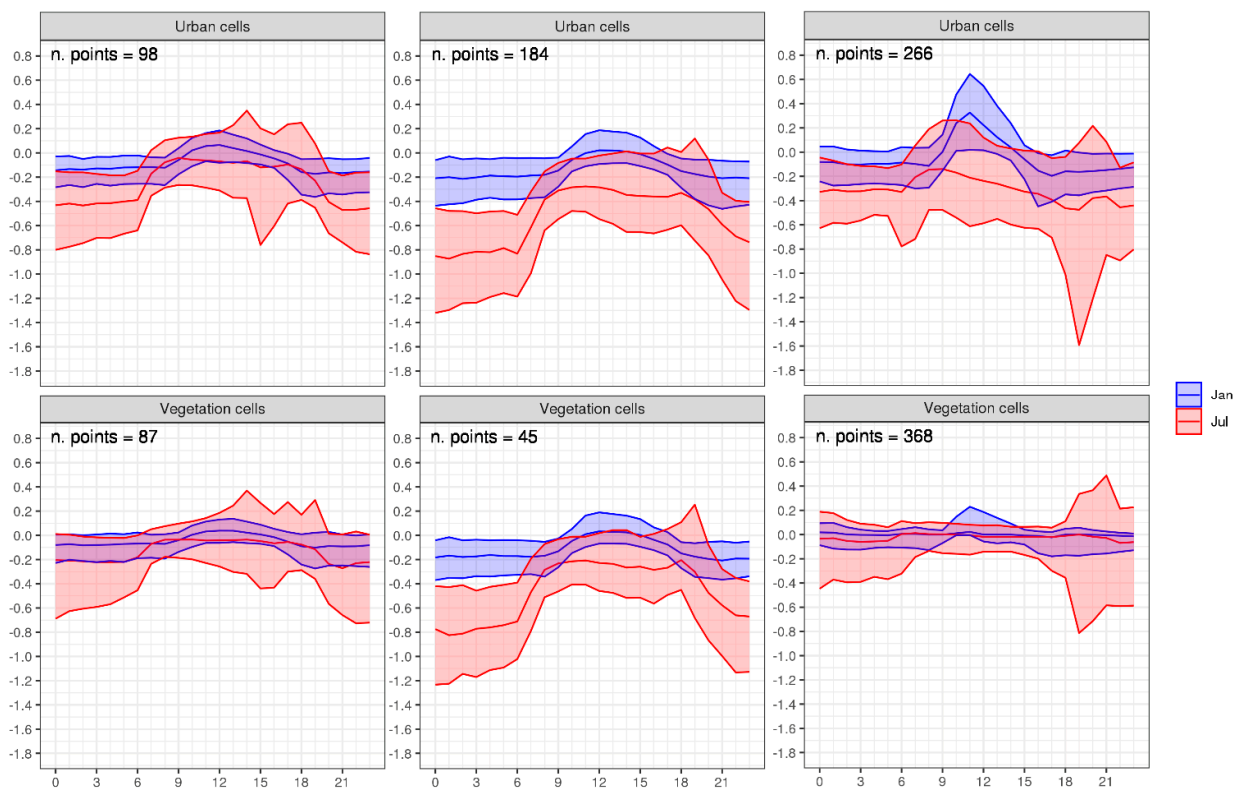


Figure 5. Daily cycle of the median, 10th, and 90th percentile temperature difference (VEG–NOVEG) within Bologna, Milano, and Madrid municipalities (left, middle, and right columns, respectively). Top row refers to quantities calculated over urban cells where vegetation fraction was removed in NOVEG simulations, while bottom row shows quantities calculated over vegetation cells where urban fraction is not prevalent and vegetation fraction was unchanged in both simulations. Colours refer to January (blue) and July (red), while shaded areas encompass the interval between 90th (upper bound) and 10th (lower bound) percentiles. Units in °C. The number of grid points associated with cell type is indicated in the panels.

Similar plots are presented for RH and WS in Figures S4 and S5, respectively. It is shown that for RH, the largest variability is observed in July and is larger in Milano and Madrid than in Bologna. The variation in RH differences can be associated, in part, to the changes observed in T but also to other parameters that are affected by vegetation, such as, among others, ground water content, heat fluxes, and precipitation. This may explain the January variability observed in Madrid urban cells vs. vegetation cells, while no great difference is observed in the temporal variations when comparing other cities and months. Concerning WS (Figure S5), the variability in the three cities is significantly less evident in January than in July, when, during the second part of the day, conspicuous differences (positive and negative) are present, likely associated with summer local circulation patterns triggered by convection, strongly affecting WS. No clear difference is noted between urban and vegetation cells for Milano and Bologna, while higher values are observed in Madrid vegetation vs. urban cells in July.

In addition to the temporal variability shown in Figure 5 for a whole city, the spatial and temporal variability in temperature differences over the grid points within the municipalities is shown in Table 3 for different averaging time periods, hourly and daily values, which are calculated considering 744 (hours in a month) and 31 (days in month) records, respectively. Taking, as reference, the monthly values (Figures 3 and 4), we note that the impact of urban vegetation on temperature in the cities can be highly variable among grid cells when looking at hourly values and daily values.

Table 3. Variability in temperature differences (VEG-NOVEG) due to vegetation and temperatures (VEG) over the municipality area. Monthly and yearly values show only the spatial variability, and the former values are representative of Figures 3 and 4. Hourly and daily values include temporal variability through min and max values, considering 744 hourly and 31 daily records per month. The bold values highlight the hourly and daily extremes: blue indicates a cooling effect (lower temperature in presence of vegetation) and red the opposite. Units are in °C.

City	Temperature		VEG-NOVEG				VEG			
	Average	Month	Minimum		Mean		Maximum		Mean	
			Min	Max	Min	Max	Min	Max	Min	Max
Bologna	hourly	January	−2.4	0.00	−0.46	0.40	−0.10	4.6	−3.2	14
		July	−5.6	0.00	−1.5	1.9	−0.13	4.5	18	33
	daily	January	−0.30	−0.10	−0.12	0.00	0.00	0.20	2.0	13
		July	−0.60	−0.20	−0.32	−0.10	0.00	0.28	23	32
	monthly	January		−0.15		−0.10		0.00		6.1
		July		−0.35		−0.20		0.00		28
	yearly			−0.25		−0.15		0.00		15.6
Milano	hourly	January	−1.7	0.00	−0.53	0.23	−0.23	1.4	−1.8	16
		July	−4.4	0.87	−1.94	2.38	−0.90	5.6	17	37
	daily	January	−0.4	−0.14	−0.20	0.00	−0.13	0.2	2.4	11
		July	−1.0	−0.35	−0.64	−0.18	−0.41	0.15	23.2	30
	monthly	January		−0.20		−0.13		−0.10		6.2
		July		−0.78		−0.50		−0.34		27.4
	yearly			−0.40		−0.28		−0.20		15.5
Madrid	hourly	January	−4.7	0.00	−0.80	0.42	0.00	2.6	−1.7	15
		July	−5.2	−0.1	−1.2	1.2	0.00	4.3	17	39
	daily	January	−0.6	−0.0	−0.10	0.0	0.00	0.43	0.48	13
		July	−1.0	−0.4	−0.30	0.0	0.00	0.44	23	32
	monthly	January		−0.25		0.00		0.23		5.3
		July		−0.57		−0.20		0.10		29
	yearly			−0.53		−0.10		0.10		16

Concerning hourly value variability, extreme temperature difference values (bold blue and red text in Table 3) are found in July for Madrid (−5.2 to +4.3 °C) and Milano (−4.4 to +5.6 °C), while Bologna presents a maximum in January (+4.6 °C, which is similar to what is found for July: +4.5 °C) and a minimum in July (−5.6 °C). When looking at daily averages, the largest variability occurs in July for Bologna (−0.60 °C to +0.28 °C) and Madrid (−1.0 to +0.44 °C), while Milano presents the maximum difference in January with +0.2 °C and the minimum in July (−1.0 °C). The alternation of hourly negative and positive values leads to a decrease in daily and, further, monthly and yearly temperature differences. It can be noted that large local hourly fluctuations are, therefore, estimated even during winter periods where the monthly average changes are rather limited.

If we look at the whole year and compare the mean temperature modelled in the three cities (VEG simulation, last column in Table 3) with the variation due to the presence of urban vegetation, we see a net cooling effect of −0.15 °C (average temperature 15.6 °C) in Bologna, −0.28 °C (15.5 °C) in Milano, and −0.10 °C (16 °C) in Madrid. Those values are significant from the perspective of climate change adaptation and mitigation efforts

when planning measures such as Nature-Based Solutions (NBSs) to limit climate-change-associated risks (Intergovernmental Panel on Climate Change, annual report 2022, [55]).

Finally, looking at the dependence of temperature differences on the vegetation fraction, Figures S6–S8 present whisker plots from hourly values for Bologna, Milano, and Madrid, respectively, as a function of the vegetation fraction for urban and vegetation cells. It is worth noting that, as mentioned before, the cell classification was performed considering the land use database information and the vegetation fraction from the actual vegetation database that was processed, as described in Section 2. Therefore, the vegetation fraction can span different values in cells with a given dominant land use other than urban. Boxes in the figures show that there is not a clear dependence of temperature differences on the vegetation fraction within the cells in the three cities. Even if, as highlighted before, the cooling effect due to the presence of urban vegetation is predominant, especially in July, the whiskers, spanning the interval 10th–90th percentile, show that, in both months, for the three cities, a strong variability is present for both positive and negative values, implying that the atmosphere interacts in a complex way with the urban texture and vegetation characteristics, such as type and distribution. Similar variability is also observed for RH (Figures S9–S11) and WS (Figures S12–S14) and, even in this case, the average effect is more pronounced in July than in January. Again, the RH and WS variability dependency on vegetation fraction or cell type is not obvious. The lack of dependency of meteorological data variability on the green area fraction assessed at the grid cell level suggests that the changes in urban atmosphere are due to the overall urban vegetation cover and, therefore, its spatial and temporal variability should be assessed at the city level to capture the variations induced by the vegetation scenario on the local circulation patterns.

4. Conclusions

This study shows how urban vegetation affects meteorological variables, such as temperature, relative humidity, and wind speed, in a city. The investigation was conducted for three cities in Southern Europe, Bologna, Milano, and Madrid, using the meteorological model WRF at 1 km resolution. The evaluation of a monthly average for January and July 2015 shows that the vegetation in urban areas is reducing the temperature and wind speed while increasing the relative humidity. The magnitude and spatial distribution of the impact depend on the season and the city; characteristics, such as the size and the morphology of the urban areas where the vegetation is distributed, as well as the local weather regime due to city's location, have an impact. Concerning the temperature, we found that a heating effect can occur, as found in localized areas in Madrid in January, and is attributable to latent heat release associated with the presence of vegetation. The analysis of the daily cycle of the temperature variations in the three cities shows that their magnitude varies within the city, depending on the cell type (urban cells or vegetation cells) and on the hour of the day. Moreover, as expected, the variability is higher in summer, when the vegetation is at its maximum activity, than in winter. The analysis showed that, sometimes, the heating effect occurs, particularly in Madrid, with a maximum around midday. In summer, large variability in temperature differences is present in all three cities, with some negative and positive extreme values occurring in the late evening and probably associated with air mass advection triggered by diurnal summer local circulation patterns causing advection from other points within the city area. Looking at the variation in meteorological parameters as a function of grid cell vegetation fraction, no clear relationship was found, while a large variability was observed in all parameters, higher in July and more dependent on cities than on urban/vegetation cell type. This result put forward the recommendation of assessing the impact of vegetation on meteorological conditions by carrying out simulations at the city level for periods of time representative of different atmospheric conditions, in order to consider all the interactions between vegetation characteristics and city morphology with atmosphere. Here, for the first time, the impact of vegetation on meteorological variables in three urban areas using real tree inventories was assessed in a realistic way. This is a fundamental step to evaluate the impact of vegetation on air quality in the three cities

considered here [29]. Overall, the results show that the long-time (monthly to yearly) mean impact of vegetation has a positive effect on the urban microclimate, decreasing temperature and increasing the humidity, while the reduction in wind speed reduces ventilation, with a potential negative impact on local pollutant emission dispersion.

The strong dependence of meteorology on vegetation and on a city's peculiarities emphasises the importance of further similar studies in other cities as a basis (i) to assess the vulnerabilities and impact of future tree planting and other kinds of Nature-Based Solutions and (ii) to improve the models' parameterisations describing the concurrent interactions between atmosphere, vegetation, and city morphology in the urban environment.

Supplementary Materials: The following supporting information can be downloaded at: <https://www.mdpi.com/article/10.3390/f14061235/s1>, Figure S1: Domains used for simulations over Italy (Milano and Bologna, left) and Spain (Madrid, right); Table S1: Domain specifications; Table S2: WRF statistical scores over Bologna, Milano and Madrid [36] computed for temperature (T), relative humidity (RH) and wind speed (WS) against local networks surface observations; Figure S2: Average difference (VEG-NOVEG) for Latent Heat Flux (LHF, W/m^2), for January (top row) and July (bottom row), referred to Bologna (left column), Milano (middle column) and Madrid (right column); Figure S3: Same as in Figure S2 but referred to Sensible Heat Flux (SHF); Figure S4: Daily cycle of the median, 10th and 90th percentiles RH difference (VEG-NOVEG) within Bologna, Milano and Madrid municipalities (left, middle and right column, respectively). Top row is referred to quantities calculated over Urban cells where vegetation fraction was removed in NOVEG simulations, while bottom row shows quantities calculated over Vegetation cells where urban fraction is not prevalent and vegetation fraction was unchanged in both simulations. Colours refer to January (blue) and July (red), while shaded areas encompass the interval between 90th (upper bound) and 10th (lower bound) percentile. Units in %. The number of grid points associated with cell type is indicated in the panels; Figure S5: Daily cycle of the median, 10th and 90th percentiles WS difference (VEG-NOVEG) within Bologna, Milano and Madrid municipalities (left, middle and right column, respectively). Top row is referred to quantities calculated over Urban cells where vegetation fraction was removed in NOVEG simulations, while bottom row shows quantities calculated over Vegetation cells where urban fraction is not prevalent and vegetation fraction was unchanged in both simulations. Colours refer to January (blue) and July (red), while shaded areas encompass the interval between 90th (upper bound) and 10th (lower bound) percentile. Units in m/s. The number of grid points associated with cell type is indicated in the panels; Figure S6: Boxplots of hourly T difference (VEG-NOVEG) as a function of vegetation fraction within the urban cells, divided into urban and vegetation cells, inside the municipality of Bologna. Whiskers span the interval 10th to 90th percentile. Blue (red) colour refers to January (July); Figure S7: Same as in Figure S6 but referred to Milano; Figure S8: Same as in Figure S6 but referred to Madrid; Figure S9: Boxplots of hourly RH difference (VEG-NOVEG) as a function of vegetation fraction within the urban cells, divided into urban and vegetation cells, inside the municipality of Bologna. Whiskers span the interval 10th to 90th percentile. Blue (red) colour refers to January (July). Units in %; Figure S10: Same as in Figure S9 but referred to Milano; Figure S11: Same as in Figure S9 but referred to Madrid; Figure S12: Boxplots of hourly wind speed (WS) difference (VEG-NOVEG) as a function of vegetation fraction within the urban cells, divided into urban and vegetation cells, inside the municipality of Bologna. Whiskers span the interval 10th to 90th percentile. Blue (red) colour refers to January (July); Figure S13: Same as in Figure S12 but referred to Milano; Figure S14: Same as in Figure S12 but referred to Madrid.

Author Contributions: Conceptualization: M.D. and M.M.; methodology: M.D., M.M. and R.B.; software: M.D., R.P., G.C. (Giuseppe Carlino), G.B., M.G.V., M.A. and D.d.I.P.; validation: M.D. and D.d.I.P.; formal analysis: M.D. and M.M.; investigation: M.D., M.M., G.B. and S.F.; resources: M.D., M.M., R.B., S.F., D.d.I.P., R.P. and M.S.; data curation: M.D., M.M., F.R., R.P., G.C. (Giuseppe Cremona) and S.F.; writing—original draft preparation: M.D. and M.M.; writing—review and editing: M.D., M.M., F.R., G.B., L.V., R.P., S.F., G.R., G.C. (Giuseppe Carlino), R.B., M.G.V., M.A. and D.d.I.P.; visualization: M.D., M.M., F.R. and G.R.; supervision: M.M. and R.B.; project administration: M.M. and G.R.; funding acquisition: M.M. All authors have read and agreed to the published version of the manuscript.

Funding: This study was developed under the project Life VEG-GAP (<https://www.lifeveggap.eu/>, accessed on 15 May 2023), which was funded by European Union Life Program in 2018, Grant Number LIFE18 PRE IT 003.

Data Availability Statement: The datasets generated during and/or analysis during the current study are not publicly available due to the high volume of data but are available from the corresponding author on reasonable request. Data analysis products are available on Information platform: <https://veggapplatform.enea.it> (accessed on 15 May 2023).

Acknowledgments: We acknowledge the support of Madrid and Milano Municipalities and of Metropolitan City of Bologna in the acquisition of tree inventories in the framework of the Life VEG-GAP project (www.lifeveggap.eu accessed on 11 June 2023). The computing resources and the related technical support used for this work were provided by CRESCO/ENEAGRID High Performance Computing infrastructure and its staff [56]. CRESCO/ENEAGRID High Performance Computing infrastructure is funded by ENEA, the Italian National Agency for New Technologies, Energy and Sustainable Economic Development and by the Italian and European research programmes, see <http://www.cresco.enea.it/english> (accessed on 14 May 2023) for information. We also acknowledge Madrid's Air Quality Service for providing meteorological dataset from the City Hall meteorological network, and ECMWF (European Centre for Medium-Range Weather Forecasts) for providing European meteorological fields (DSC-9674 Permission to use IFS data).

Conflicts of Interest: The authors declare no conflict of interest. The funders had no role in the design of the study; in the collection, analyses, or interpretation of data; in the writing of the manuscript; or in the decision to publish the results.

References

1. Perkins-Kirkpatrick, S.E.; Lewis, S.C. Increasing Trends in Regional Heatwaves. *Nat. Commun.* **2020**, *11*, 3357. [[CrossRef](#)]
2. Habeeb, D.; Vargo, J.; Stone, B. Rising Heat Wave Trends in Large US Cities. *Nat. Hazards* **2015**, *76*, 1651–1665. [[CrossRef](#)]
3. Russo, S.; Sillmann, J.; Fischer, E.M. Top Ten European Heatwaves since 1950 and Their Occurrence in the Coming Decades. *Environ. Res. Lett.* **2015**, *10*, 124003. [[CrossRef](#)]
4. Wong, K.V.; Paddon, A.; Jimenez, A. Review of World Urban Heat Islands: Many Linked to Increased Mortality. *J. Energy Resour. Technol.* **2013**, *135*, 022101. [[CrossRef](#)]
5. Robine, J.-M.; Cheung, S.L.K.; Le Roy, S.; Van Oyen, H.; Griffiths, C.; Michel, J.-P.; Herrmann, F.R. Death Toll Exceeded 70,000 in Europe during the Summer of 2003. *Comptes Rendus Biol.* **2008**, *331*, 171–178. [[CrossRef](#)]
6. Brennenstuhl, H.; Will, M.; Ries, E.; Mechler, K.; Garbade, S.; Ries, M. Patterns of Extreme Temperature-Related Catastrophic Events in Europe Including the Russian Federation: A Cross-Sectional Analysis of the Emergency Events Database. *BMJ Open* **2021**, *11*, e046359. [[CrossRef](#)]
7. Limaye, V.S.; Vargo, J.; Harkey, M.; Holloway, T.; Patz, J.A. Climate Change and Heat-Related Excess Mortality in the Eastern USA. *EcoHealth* **2018**, *15*, 485–496. [[CrossRef](#)]
8. Muthers, S.; Laschewski, G.; Matzarakis, A. The Summers 2003 and 2015 in South-West Germany: Heat Waves and Heat-Related Mortality in the Context of Climate Change. *Atmosphere* **2017**, *8*, 224. [[CrossRef](#)]
9. Urban, A.; Hanzlíková, H.; Kyselý, J.; Plavcová, E. Impacts of the 2015 Heat Waves on Mortality in the Czech Republic—a Comparison with Previous Heat Waves. *Int. J. Environ. Res. Public Health* **2017**, *14*, 1562. [[CrossRef](#)] [[PubMed](#)]
10. Michelozzi, P.; De' Donato, F.; Scortichini, M.; De Sario, M.; Asta, F.; Agabiti, N.; Guerra, R.; Martino, A.; Davoli, M. On the increase in mortality in Italy in 2015: Analysis of seasonal mortality in the 32 municipalities included in the surveillance system of daily mortality. *Epidemiol. E Prev.* **2016**, *40*, 22–28. [[CrossRef](#)]
11. Can, G.; Şahin, Ü.; Sayılı, U.; Dubé, M.; Kara, B.; Acar, H.C.; İnan, B.; Aksu Sayman, Ö.; Lebel, G.; Bustinza, R.; et al. Excess Mortality in Istanbul during Extreme Heat Waves between 2013 and 2017. *Int. J. Environ. Res. Public Health* **2019**, *16*, 4348. [[CrossRef](#)]
12. Katavoutas, G.; Founda, D. Response of Urban Heat Stress to Heat Waves in Athens (1960–2017). *Atmosphere* **2019**, *10*, 483. [[CrossRef](#)]
13. Kong, J.; Zhao, Y.; Carmeliet, J.; Lei, C. Urban Heat Island and Its Interaction with Heatwaves: A Review of Studies on Mesoscale. *Sustainability* **2021**, *13*, 10923. [[CrossRef](#)]
14. Skamarock, W.C.; Klemp, J.B.; Dudhia, J.; Gill, D.O.; Liu, Z.; Berner, J.; Wang, W.; Powers, J.J.; Duda, M.G.; Barker, D.; et al. *A Description of the Advanced Research Wrf Model VERSION 4.1*; UCAR: Boulder, CO, USA, 2019.
15. Skamarock, W.C.; Klemp, J.B.; Dudhia, J.; Gill, D.O.; Barker, D.; Duda, M.G.; Huang, X.-Y.; Wang, W.; Powers, J.J. *A Description of the Advanced Research Wrf Version 3*; UCAR: Boulder, CO, USA, 2008.
16. Du, R.; Song, J.; Huang, X.; Wang, Q.; Zhang, C.; Brousse, O.; Chan, P.W. High-Resolution Regional Modeling of Urban Moisture Island: Mechanisms and Implications on Thermal Comfort. *Build. Environ.* **2022**, *207*, 108542. [[CrossRef](#)]

17. Chen, K.; Newman, A.J.; Huang, M.; Coon, C.; Darrow, L.A.; Strickland, M.J.; Holmes, H.A. Estimating Heat-Related Exposures and Urban Heat Island Impacts: A Case Study for the 2012 Chicago Heatwave. *GeoHealth* **2022**, *6*, e2021GH000535. [CrossRef]
18. Ribeiro, I.; Martilli, A.; Falls, M.; Zonato, A.; Villalba, G. Highly Resolved WRF-BEP/BEM Simulations over Barcelona Urban Area with LCZ. *Atmos. Res.* **2021**, *248*, 105220. [CrossRef]
19. Rajeswari, J.R.; Srinivas, C.V.; Venkatraman, B. Impact of Urbanization on Boundary-Layer Parameters and Mesoscale Circulations over Tropical Coastal City, Chennai. *Meteorol. Atmos. Phys.* **2021**, *134*, 3. [CrossRef]
20. Wang, Q.; Zhang, C.; Ren, C.; Hang, J.; Li, Y. Urban Heat Island Circulations over the Beijing-Tianjin Region under Calm and Fair Conditions. *Buill. Environ.* **2020**, *180*, 107063. [CrossRef]
21. Li, H.; Zhou, Y.; Wang, X.; Zhou, X.; Zhang, H.; Sodoudi, S. Quantifying Urban Heat Island Intensity and Its Physical Mechanism Using WRF/UCM. *Sci. Total Environ.* **2019**, *650*, 3110–3119. [CrossRef]
22. Giannaros, C.; Nenes, A.; Giannaros, T.M.; Kourtidis, K.; Melas, D. A Comprehensive Approach for the Simulation of the Urban Heat Island Effect with the WRF/SLUCM Modeling System: The Case of Athens (Greece). *Atmos. Res.* **2018**, *201*, 86–101. [CrossRef]
23. Hayes, A.T.; Jandaghian, Z.; Lacasse, M.A.; Gaur, A.; Lu, H.; Laouadi, A.; Ge, H.; Wang, L. Nature-Based Solutions (NBSs) to Mitigate Urban Heat Island (UHI) Effects in Canadian Cities. *Buildings* **2022**, *12*, 925. [CrossRef]
24. Shao, H.; Kim, G. A Comprehensive Review of Different Types of Green Infrastructure to Mitigate Urban Heat Islands: Progress, Functions, and Benefits. *Land* **2022**, *11*, 1792. [CrossRef]
25. Priya, U.K.; Senthil, R. A Review of the Impact of the Green Landscape Interventions on the Urban Microclimate of Tropical Areas. *Buill. Environ.* **2021**, *205*, 108190. [CrossRef]
26. Liao, W.; Guldmann, J.-M.; Hu, L.; Cao, Q.; Gan, D.; Li, X. Linking Urban Park Cool Island Effects to the Landscape Patterns inside and Outside the Park: A Simultaneous Equation Modeling Approach. *Landsc. Urban Plan.* **2023**, *232*, 104681. [CrossRef]
27. Helletsgruber, C.; Gillner, S.; Gulyás, Á.; Junker, R.R.; Tanács, E.; Hof, A. Identifying Tree Traits for Cooling Urban Heat Islands—A Cross-City Empirical Analysis. *Forests* **2020**, *11*, 1064. [CrossRef]
28. Eckmann, T.; Morach, A.; Hamilton, M.; Walker, J.; Simpson, L.; Lower, S.; McNamee, A.; Haripriyan, A.; Castillo, D.; Grandy, S.; et al. Measuring and Modeling Microclimate Impacts of Sequoiadendron Giganteum. *Sustain. Cities Soc.* **2018**, *38*, 509–525. [CrossRef]
29. Mircea, M.; Borge, R.; Finardi, S.; Russo, F.; de la Paz, D.; D'Isidoro, M.; Cremona, G.; Villani, M.G.; Cappelletti, A.; Adani, M.; et al. The Role of Vegetation on Urban Atmosphere of Three European Cities. Part 2: Evaluation of Vegetation Impact on Air Pollutant Concentrations and Depositions. *Forests* **2023**. submitted.
30. NOAA National Centers for Environmental Information. State of the Climate: Global Climate Report for Annual 2020, Published Online. 2021. Available online: <https://www.ncdc.noaa.gov/sotc/global/202013> (accessed on 25 February 2022).
31. Kennedy, J.; Morice, C.; Parker, D.; Kendon, M. Global and Regional Climate in 2015. *Weather* **2016**, *71*, 185–192. [CrossRef]
32. Bessagnet, B.; Pirovano, G.; Mircea, M.; Cuvelier, C.; Aulinger, A.; Calori, G.; Ciarelli, G.; Manders, A.; Stern, R.; Tsyro, S.; et al. Presentation of the EURODELTA III Intercomparison Exercise—Evaluation of the Chemistry Transport Models' Performance on Criteria Pollutants and Joint Analysis with Meteorology. *Environ. Res. Lett.* **2016**, *16*, 12667–12701. Available online: <https://acp.copernicus.org/articles/16/12667/2016/acp-16-12667-2016-metrics.html> (accessed on 11 June 2023). [CrossRef]
33. Rasilla, D.; Allende, F.; Martilli, A.; Fernández, F. Heat Waves and Human Well-Being in Madrid (Spain). *Atmosphere* **2019**, *10*, 288. [CrossRef]
34. Simmonds, A.J. Trends in the Tropospheric General Circulation from 1979 to 2022. *Weather Clim. Dyn.* **2022**, *3*, 777–809. [CrossRef]
35. World Meteorological Organization. WMO Global to Annual Climate Update. Target Years: 2023 and 2023–2027; WMO: Geneva, Switzerland, 2023. Available online: https://library.wmo.int/doc_num.php?explnum_id=11629 (accessed on 11 June 2023).
36. De la Paz, D.; de Andrés, J.M.; Narros, A.; Silibello, C.; Finardi, S.; Fares, S.; Tejero, L.; Borge, R.; Mircea, M. Assessment of Air Quality and Meteorological Changes Induced by Future Vegetation in Madrid. *Forests* **2022**, *13*, 690. [CrossRef]
37. Büttner, G. CORINE Land Cover and Land Cover Change Products. In *Land Use and Land Cover Mapping in Europe. Remote Sensing and Digital Image Processing*; Manakos, I., Braun, M., Eds.; Springer: Dordrecht, Germany, 2014; Volume 18, pp. 55–74, ISBN 978-94-007-7969-3.
38. Martilli, A.; Clappier, A.; Rotach, M.W. An Urban Surface Exchange Parameterisation for Mesoscale Models. *Bound. Layer Meteorol.* **2002**, *104*, 261–304. [CrossRef]
39. Hong, S.Y.; Lim, J.-O.J. The WRF Single-Moment 6-Class Microphysics Scheme (WSM6). *J. Kor. Meteorol. Soc.* **2006**, *42*, 129–151.
40. Janjić, Z.I. The Step-Mountain Eta Coordinate Model: Further Developments of the Convection, Viscous Sublayer, and Turbulence Closure Schemes. *Mon. Weather Rev.* **1994**, *122*, 927–945. [CrossRef]
41. Bougeault, P.; Lacarrere, P. Parameterization of Orography-Induced Turbulence in a Mesobeta-Scale Model. *Mon. Weather Rev.* **1989**, *117*, 1872–1890. [CrossRef]
42. Janjić, Z.I. *The Surface Layer in the NCEP Eta Model*; American Meteor Society: Norfolk, VA, USA, 1996; pp. 354–355.
43. De la Paz, D.; Borge, R.; Martilli, A. Assessment of a High Resolution Annual WRF-BEP/CMAQ Simulation for the Urban Area of Madrid (Spain). *Atmos. Environ.* **2016**, *144*, 282–296. [CrossRef]
44. Liu, Y.; Chen, F.; Warner, T.; Basara, J. Verification of a Mesoscale Data-Assimilation and Forecasting System for the Oklahoma City Area during the Joint Urban 2003 Field Project. *J. Appl. Meteorol. Climatol.* **2006**, *45*, 912–929. [CrossRef]

45. Iacono, M.J.; Delamere, J.S.; Mlawer, E.J.; Shephard, M.W.; Clough, S.A.; Collins, W.D. Radiative Forcing by Long-Lived Greenhouse Gases: Calculations with the AER Radiative Transfer Models. *J. Geophys. Res. Atmos.* **2008**, *113*. [[CrossRef](#)]
46. Fels, S.B.; Schwarzkopf, M.D. An Efficient, Accurate Algorithm for Calculating CO₂ 15 Mm Band Cooling Rates. *J. Geophys. Res. Ocean.* **1981**, *86*, 1205–1232. [[CrossRef](#)]
47. Dudhia, J. Numerical Study of Convection Observed during the Winter Monsoon Experiment Using a Mesoscale Two-Dimensional Model. *J. Atmos. Sci.* **1989**, *46*, 3077–3107. [[CrossRef](#)]
48. Hersbach, H.; Bell, B.; Berrisford, P.; Hirahara, S.; Horányi, A.; Muñoz-Sabater, J.; Nicolas, J.; Peubey, C.; Radu, R.; Schepers, D.; et al. The ERA5 Global Reanalysis. *Q. J. R. Meteorol. Soc.* **2020**, *146*, 1999–2049. [[CrossRef](#)]
49. Emery, C.; Tai, E.; Yarwood, G. *Enhanced Meteorological Modeling and Performance Evaluation for Two Texas Ozone Episodes*; ENVIRON International Corporation: Novato, CA, USA, 2001. Available online: <https://wayback.archive-it.org/414/20210529063824/https://www.tceq.texas.gov/assets/public/implementation/air/am/contracts/reports/mm/EnhancedMetModelingAndPerformanceEvaluation.pdf> (accessed on 11 June 2023).
50. Tesche, T.W.; Tremback, C.J. Operational Evaluation of the MM5 Meteorological Model over the Continental United States: Protocol for Annual and Episodic Evaluation. 2002. Available online: https://www.epa.gov/sites/default/files/2020-10/documents/tesche_2002_evaluation_protocol.pdf (accessed on 15 May 2023).
51. R Core Team. *R: A Language and Environment for Statistical Computing*; R Foundation for Statistical Computing: Vienna, Austria, 2021. Available online: <https://www.r-project.org/> (accessed on 11 June 2023).
52. Wickham, H.; Averick, M.; Bryan, J.; Chang, W.; McGowan, L.D.; François, R.; Grolemund, G.; Hayes, A.; Henry, L.; Hester, J.; et al. Welcome to the Tidyverse. *J. Open Source Softw.* **2019**, *4*, 1686. [[CrossRef](#)]
53. Robotto, A.; Barbero, S.; Cremonini, R.; Brizio, E. Improving Air Quality and Health in Northern Italy: Limits and Perspectives. *medRxiv* **2022**. [[CrossRef](#)]
54. Masiol, M.; Squizzato, S.; Formenton, G.; Khan, M.B.; Hopke, P.K.; Nenes, A.; Pandis, S.N.; Tositti, L.; Benetello, F.; Visin, F.; et al. Hybrid Multiple-Site Mass Closure and Source Apportionment of PM_{2.5} and Aerosol Acidity at Major Cities in the Po Valley. *Sci. Total Environ.* **2020**, *704*, 135287. [[CrossRef](#)] [[PubMed](#)]
55. Bednar-Friedl, B.; Biesbroek, R.; Schmidt, D.N.; Alexander, P.; Børshiem, K.Y.; Carnicer, J.; Georgopoulou, E.; Haasnoot, M.; Le Cozannet, G.; Lionello, P.; et al. Contribution of Working Group II to the Sixth Assessment Report of the Intergovernmental Panel on Climate Change. In *Climate Change 2022: Impacts, Adaptation and Vulnerability*; Pörtner, H.-O., Roberts, D., Tignor, M., Poloczanska, E., Mintenbeck, K., Alegria, A., Craig, M., Langsdorf, S., Löschke, S., Möller, V., et al., Eds.; Cambridge University Press: Cambridge, UK; New York, NY, USA, 2022; pp. 1817–1927.
56. Iannone, F.; Ambrosino, F.; Bracco, G.; De Rosa, M.; Funel, A.; Guarnieri, G.; Migliori, S.; Palombi, F.; Ponti, G.; Santomauro, G.; et al. CRESCO ENEA HPC Clusters: A Working Example of a Multifabric GPFS Spectrum Scale Layout. In *Proceedings of the 2019 International Conference on High Performance Computing Simulation (HPCS)*, Dublin, Ireland, 15–19 July 2019; pp. 1051–1052.

Disclaimer/Publisher’s Note: The statements, opinions and data contained in all publications are solely those of the individual author(s) and contributor(s) and not of MDPI and/or the editor(s). MDPI and/or the editor(s) disclaim responsibility for any injury to people or property resulting from any ideas, methods, instructions or products referred to in the content.